mathematics

MDPI

Article

Criteria-Based Model of Hybrid Photovoltaic–Wind Energy System with Micro-Compressed Air Energy Storage

Georgios E. Arnaoutakis [1,*], Gudrun Kocher-Oberlehner [2] and Dimitris Al. Katsaprakakis [1]

[1] Department of Mechanical Engineering, Hellenic Mediterranean University, 71410 Heraklion, Greece
[2] Engineering Department, University College Roosevelt, Lange Noordstraat 1, P.O. Box 94, 4331 CB Middelburg, The Netherlands
* Correspondence: arnaoutakis@hmu.gr

Abstract: Utilization of solar and wind energy is increasing worldwide. Photovoltaic and wind energy systems are among the major contributing tec4hnologies to the generation capacity from renewable energy sources; however, the generation often does not temporally match the demand. Micro-compressed air energy storage (micro-CAES) is among the low-cost storage options, and its coupling with the power generated by photovoltaics and wind turbines can provide demand shifting, modeled by efficient algorithms. A model based on criteria that are preset according to the demand is presented. The model decides on the distribution of the generated energy, depending on the state of the energy storage and the preset criteria of each storage technology. The satisfaction of the demand by the energy production and micro-CAES is compared to that of storage batteries. The demand originates in a case study of a household and optimal configurations of photovoltaics and wind turbines, and the storage capacities and costs are compared. An optimal configuration of 30 photovoltaic panels and two wind turbines was found for micro-CAES. The annual stored energy of micro-CAES was 114 kWh higher than that of the system with batteries.

Keywords: photovoltaics; wind energy; compressed air; energy storage; algorithms

MSC: 37M10

check for updates

Citation: Arnaoutakis, G.E.; Kocher-Oberlehner, G.; Katsaprakakis, D.A. Criteria-Based Model of Hybrid Photovoltaic–Wind Energy System with Micro-Compressed Air Energy Storage. *Mathematics* **2023**, *11*, 391. https://doi.org/10.3390/math11020391

Academic Editors: Theodore E. Simos and Charampos Tsitouras

Received: 31 October 2022
Revised: 9 December 2022
Accepted: 6 January 2023
Published: 11 January 2023

Copyright: © 2023 by the authors. Licensee MDPI, Basel, Switzerland. This article is an open access article distributed under the terms and conditions of the Creative Commons Attribution (CC BY) license (https://creativecommons.org/licenses/by/4.0/).

1. Introduction

Energy production from renewable energy resources is increasing in capacity worldwide [1]. Although this energy transition is very favorable for the reduction of carbon emissions, it is still limited by the intermittency of renewable energy resources, such as solar energy and wind energy. The combined operation of suitable technologies—such as a concentrated solar power (CSP) tower and a parabolic trough [2] or hybrid CSP-photovoltaic plants [3]—is one solution to the intermittency problem. Alternatively, energy storage may be used to compensate for intermittency on multi-hour temporal scales. Energy storage is one of the main ways of circumventing this intermittency limitation for multi-hour temporal scales. Thermal storage is one of the low-cost energy storage technologies, with significant developm4ents in materials and systems [4,5] to reduce the costs even further; however, while this storage option is suitable for the storage of thermal energy, it is not suitable for storing electricity generated by the major renewable energy technologies, i.e., photovoltaic solar cells [6] and wind turbines [7]. Storage in batteries is one option toward this end; however, it suffers from higher costs, due to the limited number of cycles of the current state of the technology, which leads to replacement after 10 years of operation [8].

A low-cost energy storage technology is compressed air energy storage (CAES). Several large-scale CAES projects have been implemented around the world. The first facility was the Huntorf plant near Bremen, Germany, which was built in 1978 with a capacity of 290 MW and a total storage volume of 310,000 m^3. The Huntorf plant was built to provide up to 4 h of backup power and operated at 90% availability and 99% starting reliability [9,10].

The second large scale plant was the 110 MW McIntosh plant in Alabama, USA, with a total storage volume of 560,000 m^3. It was designed to generate at full power for 26 h and was further modeled to couple energy produced by photovoltaic power plants [11]. The specific setup costs of the Huntorf and McInstosh plants were USD 143/kWh and USD 24/kWh, respectively [10]. Numerous adiabatic CAES plants have been proposed, as well as liquid air energy storage; however, little analysis of their specific costs is available [12].

The main constraint and the most important component related to the development of CAES is the volume for storing the compressed air [13]. Although salt domes or saline caverns have been tested for several years in CAES plants, certain issues require further consideration. One issue is the reaction of salt solutions to the surroundings, with subsequent abrasion of the saline cavern. Another major issue is the mixing of the solutions with the compressed air that can resu4lt in corrosion of the plant components, such as the turbine, the valves, or the pipes. The effects of corrosion can be significantly increased with the presence of moisture, especially in the case of high pressure and high temperature, [14].

Aquifers, with the ability of a constant pressure system utilizing the incompressibility of water [13] and a relatively low cost of development [14], were considered for underground storage. According to an ESPC study, the estimated capital cost of a CAES plant, without salt storage, is higher than the capital cost of a plant utilizing an aquifer energy storage [15].

Large-scale CAES plants are limited to certain locations. This holds true for salt domes or salt beds; however, aquifer systems are located in several areas around the world [16]. Many of these aquifers extend to more than one country, over several hundreds of kilometers.

A 270 MW CAES plant was planned in the Iowa Stored Energy Park, to make use of underground aquifers. The underground geology of the selected site met the requisite parameters for an efficient and stable CAES system. The aquifer is surrounded by porous sandstone, which in turn is surrounded by impermeable cap rock. The project was designed for the storage of electricity generated from nearby wind farms by 2011 and was estimated to have provided 268 MW of electrical power to the grid for 16 h, but it was terminated due to geological limitations [17].

Micro-CAES

The size of the demonstrated plants brought CAES into maturity as a reliable storage technology. The main constraint is CAES's dependence on the size and geology of the underground caverns. In places lacking suitable geology, micro-CAES is considered for distributed generation [18].

A number of companies and manufacturers produce micro-CAES systems for industrial or residential use. One of these companies manufactures a complete uninterruptible power supply (UPS) system that is comprised of commercial compressed air tanks, a thermal storage unit, a small turbine/alternator, and a continuously spinning flywheel. The system, called thermal and compressed air storage (TACAS), provides running times of 30 min, which can supply enough backup power for the runtime requirements of 90% of organizations [19]. The lifespan of the system is guaranteed for more than 20 years, which is more than twice the lifespan of a battery storage system [20]. A small-scale compressed air energy storage (SSCAES) system was reported for an industrial facility in Ontario, Canada. The concept is primarily based on the storage of compressed air in high pressure vessels [21]. The system comprises one or more 2 to 10 MW CAES units, depending on the demand of4 the facility.

According to estimations, if the micro-CAES system is combined with wind turbines, it can provide 4 h of power generation by utilizing 8 h of air compression per day [15]. The system can also be integrated with landfill gas (LFG) or biogas [22] facilities by utilizing 12 and 24 h of air and gas compression per day, respectively, to supply another 4 h of power generation per day [15]. A micro-CAES system includes air compressors that share functionality with cryogenic facilities, as well as in combination with renewable

technologies for power generation [18]. In this paper, a criteria-based model for storing energy generated by photovoltaics and wind turbines in micro-CAES is presented. The generated energy is demonstrated by a case study in a small residence, covering the energy demand over an entire year.

2. Materials and Methods

2.1. Modeled System

The developed simulation model is depicted in Figure 1 and consists of the following components:

- Monocrystalline silicon solar panels (solar energy power plus SE-185M24/F) were utilized, with a peak power of 185 W and efficiency of 13%;
- A 1 kW wind turbine (Foshan OUYAD FD3.0-1000) with cut-in wind speed of 2 m/s;
- AGM-type batteries (Effekta, BTL 12–200 12 V/200 Ah) with an efficiency of 85%;
- A charge controller (Phocos CXN 40 A) for both systems;
- An AC inverter (Cotek 300 W/24 V) with 5.75 kW power and 90% efficiency;
- A CAES system consisting of air stor14ge operating between 1 and 10 m^3 at a compression ratio of 15 with a total charge/discharge time of 5/1 h and mechanical storage efficiency of 48% [20,23].

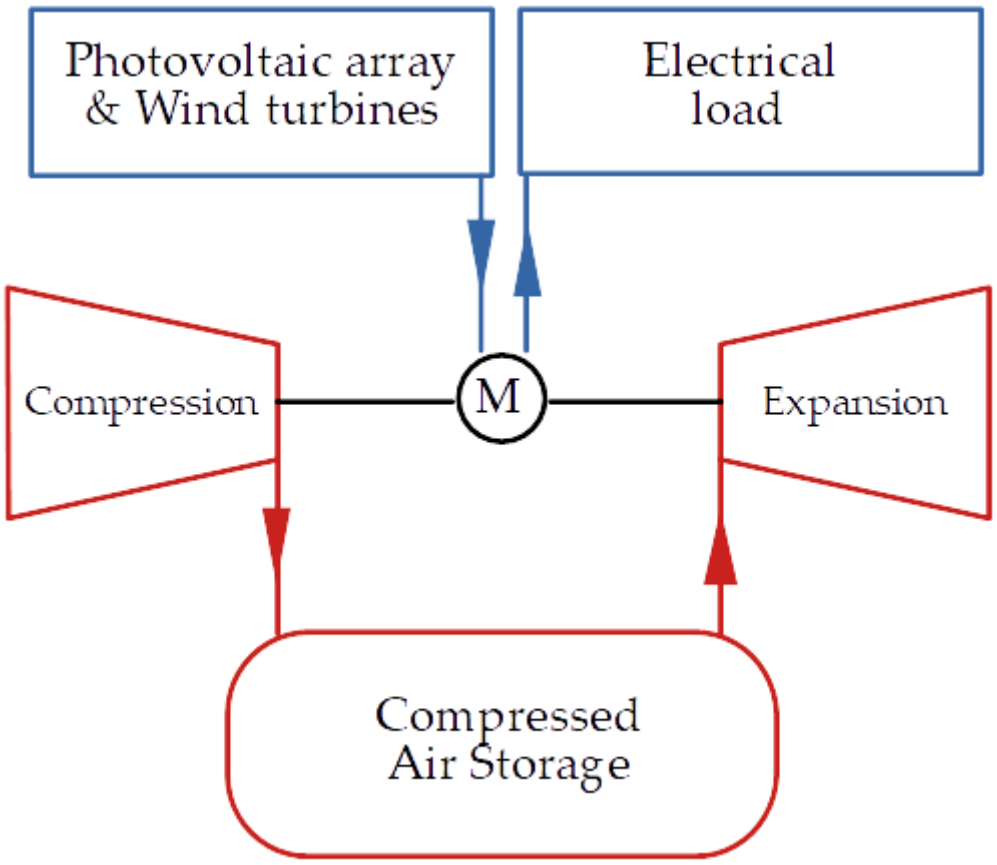

Figure 1. Schematic of modeled system. Power lines are colored blue, while the air compression and expansion cycle are colored red.

2.2. Sizing of the System

All the system inputs, along with the solar and wind resource data, were sequentially computed for the time j of the year. Hourly time steps were considered here; however, different intervals could be utilized according to the requirements of the system.

The energy production $E_{PV}(j)$ from the PV system at the time j of the year was calculated as

$$E_{PV}(j) = S \times (\eta r\,[1 - ßp(Tc - Tr)]) \times G(j) \quad (1)$$

where G(j) is the irradiation at the time j of the year, S is the area of the PV, ηr is the efficiency of the PV at temperature Tr = 25 °C, ßp is the temperature rate performance of the system, and Tc is the temperature of the system. Tc is associated with the environment temperature Ta, according to the Evans equation [9]:

$$Tc - Ta = (219 + 832K'_T) \times (NOCT - 20)/800 \quad (2)$$

where NOCT is the nominal operating cell temperature and K'_T is the average monthly cloud index. PVsyst was used to obtain the average monthly cloud index. The irradiance at the optimum angle was estimated from measurements of the horizontal irradiance by applying the following factor:

$$Cf = 1 - 1.17 \times 10^{-4}\,(\varphi_{opt} - \varphi)^2 \quad (3)$$

where φ_{opt} = the optimum tilt angle (31°) and φ = the actual angle (0°). Linear degradation losses were considered as 0.7% per year [24]; however, recent analysis [25,26] indicates that the degradation rate is often nonlinear.

Building-integrated wind turbines (WT) are installed at a height U_Z that is different from the wind measurements. The wind power law was used to transfer the given wind data at 10 m to the desired hub height [27]:

$$U_Z = U_R \times [(\ln Z/Z_0)/(\ln Z_R/Z_0)] \quad (4)$$

where Z = hub height, Z_R = current height, Z_0 = surface roughness, and U_R = wind speed at current height at time (j).

The energy production from the wind turbine $E_{WT}(j)$ at the time j of the year was calculated as

$$E_{WT}(j) = P \times N \times H \quad (5)$$

where P is the power produced by the turbine at the height-corrected wind speed, N is the number of wind turbines, and H is the hour of the day.

The work Wc used by the compressor of the system is calculated as

$$W_{comp} = m_{air} \times \Delta h_{comp} \quad (6)$$

where a mass flow rate of m_{air} of 0.024 kg/s is used by the compressor. The change in enthalpy Δh_{comp} was calculated as

$$\Delta h_{comp} = c_{p1\text{-}2} \times (T_2 - T_1)/\eta_c \quad (7)$$

where the capacity $c_{p1–2}$ and temperatures T_1 and T_2 of the isentropic process are calculated as

$$c_{p1\text{-}2} = a + b \times T_1 \quad (8)$$

$$T_2 = T_1 \times (P_2/P_1)^{k-1/k} \quad (9)$$

The work W_{exp} at the expansion phase was calculated as

$$W_{exp} = m_{air} \times \Delta h_{exp} \quad (10)$$

while the change in enthalpy Δh_{exp} can be calculated as

$$\Delta h_{exp} = c_{p3\text{-}4} \times (T_3 - T_4)/\eta_c \quad (11)$$

where the capacity $c_{p3–4}$ and temperatures T_3 and T_4 of the isentropic process are calculated as

$$c_{p3\text{-}4} = a + b \times T_1 \tag{12}$$

$$T_4 = T_3 \times (P_3/P_4)^{k-1/k} \tag{13}$$

An isentropic efficiency η_c of 0.8 was used in the compression and expansion phases.

2.3. System Simulation

The following algorithm has been applied in the prediction of photovoltaic generators with Markov chains [28], and it was adopted to include the generation from the wind turbine and the CAES system. The algorithm follows decision routines as applied to combined concentrating solar power plants [7,29], while ranking according to information of tariff can be introduced with optimum prioritization models [30].

The algorithm that determines the loss of load probability (LOLP) satisfies the following inequality for each hour of the day:

The calculation of the energy load demand $E_{dem}(j)$ initially examines whether the load is met by the produced energy E(j) before being supplied to the user $E_{user}(j)$, or is not met as $E_U(j)$; therefore:

$$\text{if } E(j) \geq E_{dem}(j)/\eta_{inv} \text{ then } E_{user}(j) = E_{dem}(j) \text{ and } E_U(j) = 0 \tag{14}$$

In case the demand is met by the produced energy, the stored energy E_S is calculated as

$$E_S(j) = E(j) - (Ed(j)/\eta_{inv}) \tag{15}$$

For this reason, the state of storage (SOS) at hour j, depending on its efficiency η_{bat} and its capacity C_B between its states Ebmax and Eb, are examined:

$$\begin{gathered}\text{if SOS(j)} < \text{Ebmax then } E_B(j+1) = \min(E_B(j) + Es(j) \times \eta_{bat} \\ \text{and SOS(j + 1)} = EB(j+1) \times 100/C_B\end{gathered} \tag{16}$$

In the alternative case, the energy $E_{unused}(j)$ is not used; that is:

$$\text{else } E_{unused}(j) = Es(j) \tag{17}$$

If the demand is not met, the state of the storage is examined; that is:

$$\text{if SOS(j)} > E_{Bmin} \text{ then} \tag{18}$$

$$\text{if } E(j) + [E_B(j) - C_B \times (1 - DOD))] \geq E_{dem}(j)/\eta_{inv} \text{ then } E_{user}(j) = E_{dem}(j) \Rightarrow E_U(j) = 0 \tag{19}$$

the demand is met and the storage is discharging; that is:

$$E_B(j+1) = \max[E_B(j) + E(j) - E_{dem}(j)/\eta_{inv}] \text{ and } \max[C_B \times (1 - DOD)] \tag{20}$$

Otherwise, the demand is not met, which means that the storage is empty; that is:

$$E_U(j) = E_{dem}(j) \tag{21}$$

In that case,

$$\text{if } E(j) > 0 \text{ then } Es(j) = E(j) \tag{22}$$

and the storage is charging; that is:

$$E_B(j+1) = E_B(j) + E_S(j) \times \eta_{bat} \text{ and SOS(j + 1)} \times 100/C_B \tag{23}$$

2.4. Cost Analysis

Capital cost includes the costs of each component, i.e., PV panels, wind turbines, the inverter, the charge controller, mounting, and wiring, as well as labor/installation costs.

Since operation and maintenance (O&M) is an important cost factor in any power generation system, the analysis also includes the replacement cost of the balance of system (BOS) components over the lifetime of the system.

All the components' costs were calculated after market research. A 5-year period was assumed to be the maximum for battery operation, so four replacements during 20 years were taken into account. The inverter and the charge controller were also considered for replacement after ten years of operation.

2.5. Case Study

An investigation was carried out to identify the average energy consumption of a four-member residence, based on a stand-alone photovoltaic system [28]. The average daily energy consumption of the household was estimated to be 9.71 kWh. An economic energy-consumption profile, in terms of energy-saving appliances, light bulbs, ceiling fans, double-framed walls, and insulation, was assumed. The average monthly solar irradiance in the location (latitude: 35°19 N, longitude: 25°40 E) of the case study, according to the photovoltaic geographical information system [31], is displayed in Figure 2.

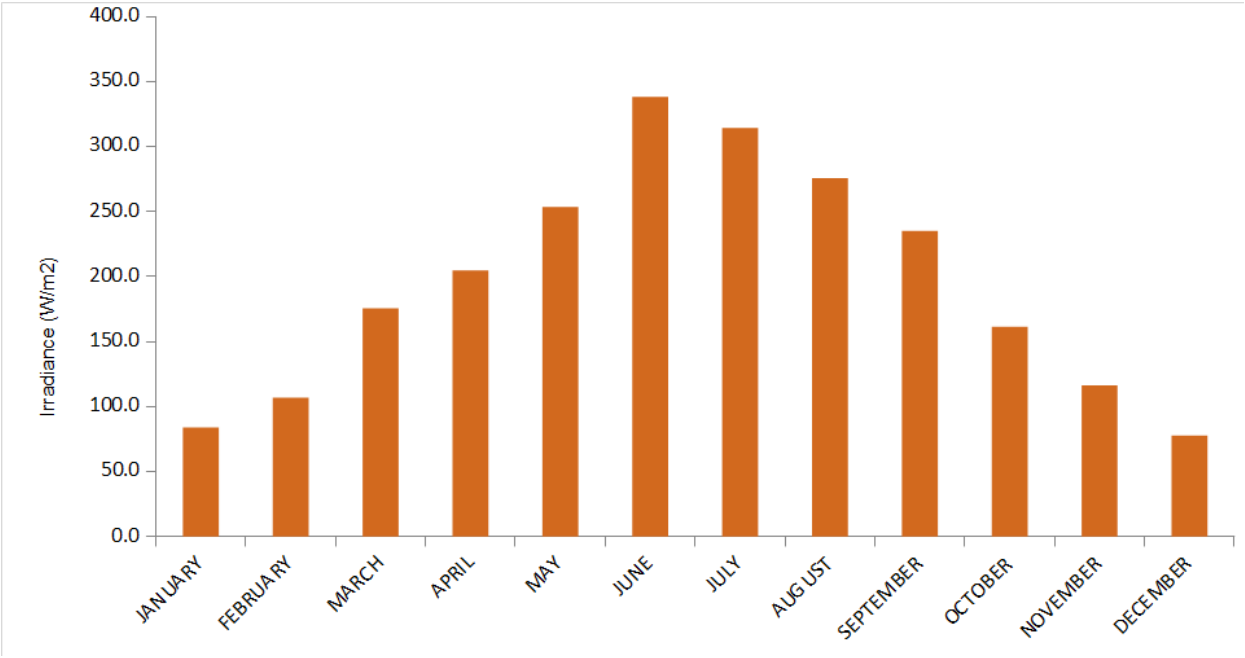

Figure 2. Average monthly solar irradiance used in the case study.

Similar systems were compared previously [32] for Mediterranean areas, leading to the conclusion that hybrid photovoltaic/wind systems do not offer high availability due to the low wind potential observed in the examined area. The chosen location was not considered ideal in comparison to other areas because of the low yearly average wind speed of 2 m/s. Figure 3 shows the wind statistics based on the measurements taken for each month of the year from weather stations in Crete. The highest annual probability occurs at 3 m/s, which is in reasonable agreement with the probability density of the location [33].

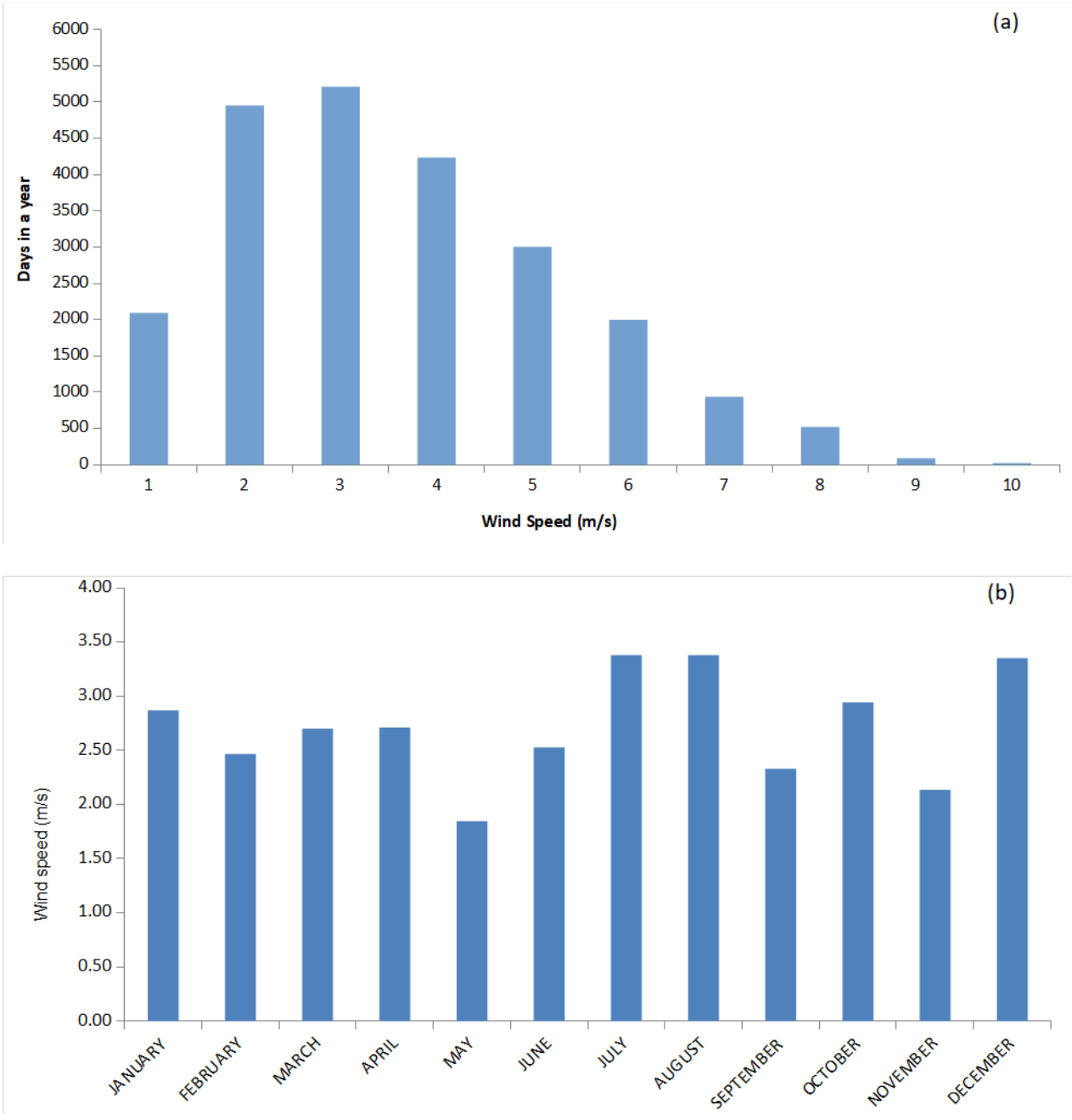

Figure 3. (**a**) Histogram of wind speed (m/s) vs. days of year and (**b**) average monthly wind speed (m/s) used in the case study.

3. Results

The algorithm presented in Section 2 was computed iteratively for a number of different sizings of the hybrid system. For each iteration, the number of generators—that is, photovoltaic panels and wind turbines—and the stored energy (i.e., the number of batteries and the volume of the micro-CAES) were the independent variables. The generated energy, the stored energy, the energy supplied to the user, and the unsatisfied energy were calculated.

3.1. Scenarios of the Investigated Systems

Optimum combinations of the hybrid system were implemented in order to provide the daily demand, with a criteria of an acceptable LOLP at 2% and minimum costs. Table 1 presents the scenarios that fulfilled the set of criteria for a hybrid system with batteries,

while Table 2 presents the respective scenarios with the micro-CAES system. The number of photovoltaic panels was limited to 40, in accordance with space limitations in roof installations at domestic residences and corresponding to approximately 50 m^2. The number of wind turbines in the scenarios was limited to three, in accordance with low noise levels for residential areas. The optimal configurations consisted of 30 photovoltaic panels and two wind turbines, exhibiting 1.99% and 1.98% LOLP with battery and micro-CAES systems, respectively.

Table 1. Scenarios of hybrid system with batteries satisfying the preset criteria.

Scenario	PV	WT	Battery	LOLP (%)	E_{unused} (kWh)
B-1	40	1	23	1.95%	172.39
B-2	30	1	27	1.97%	189.54
B-3	30	2	11	1.99%	168.46
B-4	20	2	17	1.90%	160.75
B-5	15	3	10	1.97%	157.76

Table 2. Scenarios of hybrid system with micro-CAES satisfying the preset criteria.

Scenario	PV	WT	μ-CAES (Wh)	LOLP (%)	E_{unused} (kWh)
C-1	40	1	9840	1.84%	406.84
C-2	30	1	10,320	1.90%	444.81
C-3	30	2	7920	1.98%	328.35
C-4	20	2	8640	1.86%	345.02
C-5	15	3	7440	1.94%	289.62

Table 3 presents the main annual power demand and production statistics.

Table 3. Essential annual power demand and production statistics of the hybrid system.

Annual Demand Statistics	
Annual peak power demand (kW)	2.63
Annual minimum power demand (KW)	0.20
Annual electricity consumption (MWh)	4.77
Average daily consumption (kWh)	9.71
Annual Production Statistics	
Annual wind turbine production (MWh)	3.78
Annual photovoltaics production (MWh)	8.08
Annual unsatisfied energy (MWh)	0.32
Annual energy supplied to the user (MWh)	2.14
Annual unused energy (MWh)	6.88
Total production (MWh)	11.87

3.2. Generated Electrical Energy

The monthly energy produced by each system can be seen in Figure 4. The majority of the produced electricity is generated by the photovoltaics, with higher production between May and September, while the electricity production of the wind turbine is higher during December and January.

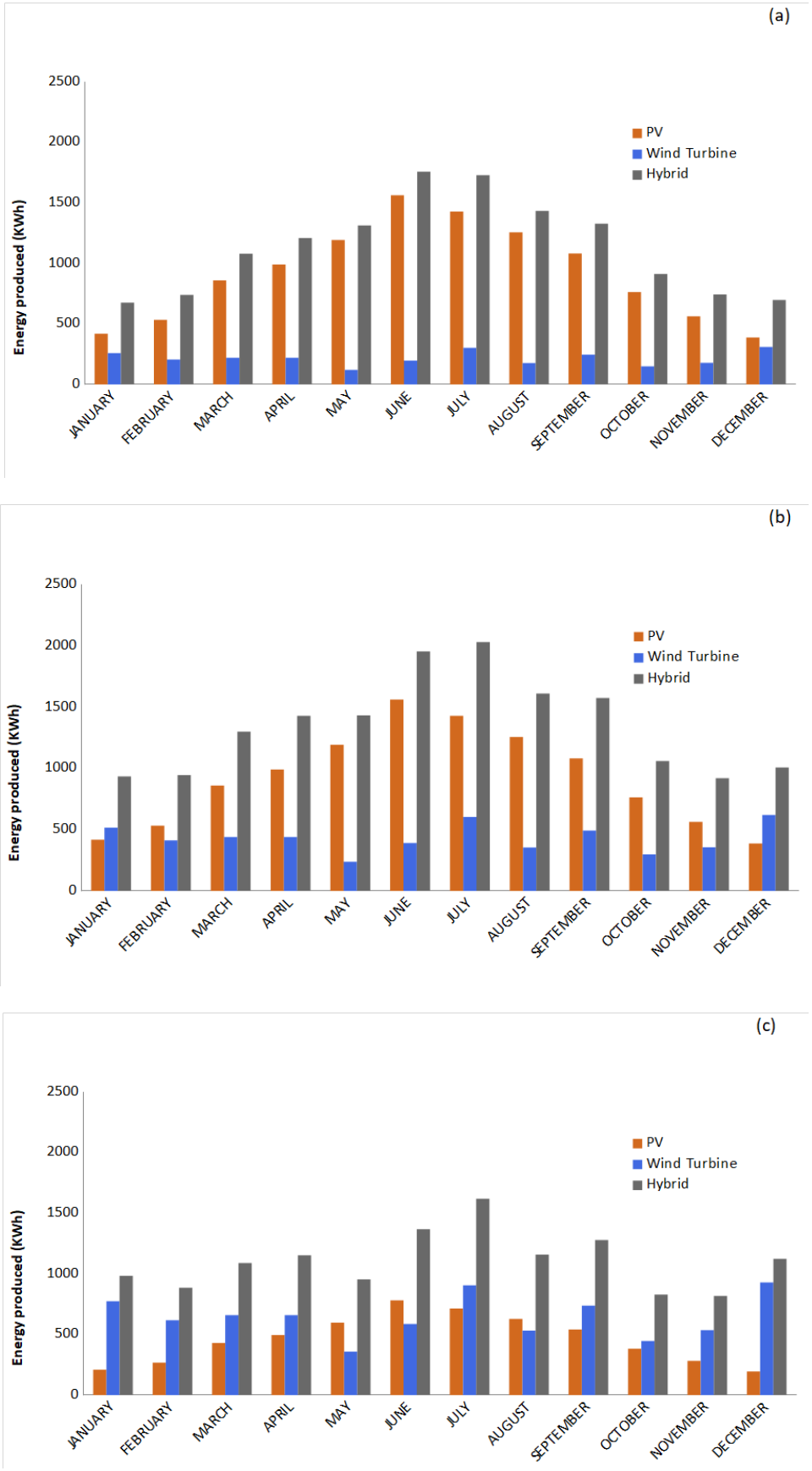

Figure 4. Monthly energy production of the photovoltaics, wind, and hybrid systems for scenarios (**a**) C-2, (**b**) C-3, and (**c**) C-5.

The monthly produced electricity by the optimal configuration of photovoltaics, wind turbine, and the overall hybrid system, along with the solar irradiance and the wind speed, are tabulated in Table 4. The hourly time series of energy produced by each system is shown in Figure 5.

Table 4. Average monthly solar and wind resource for energy production of the optimal system [1].

Month	Gh (W/m^2)	Ws (m/s)	PV (Wh)	WT (Wh)	Hybrid (Wh)
Jan	84.0	2.87	418	516	934
Feb	107.0	2.47	533	412	945
Mar	175.7	2.70	860	439	1299
Apr	204.8	2.71	991	439	1428
May	253.7	1.85	1193	239	1432
Jun	338.1	2.53	1562	391	1953
Jul	314.4	3.38	1428	603	2031
Aug	275.9	3.38	1257	354	1611
Sep	235.1	2.33	1081	492	1574
Oct	161.5	2.94	763	297	1060
Nov	116.4	2.13	563	357	921
Dec	77.8	3.35	388	619	1007

[1] The system consists of 30 photovoltaic solar panels and two wind turbines.

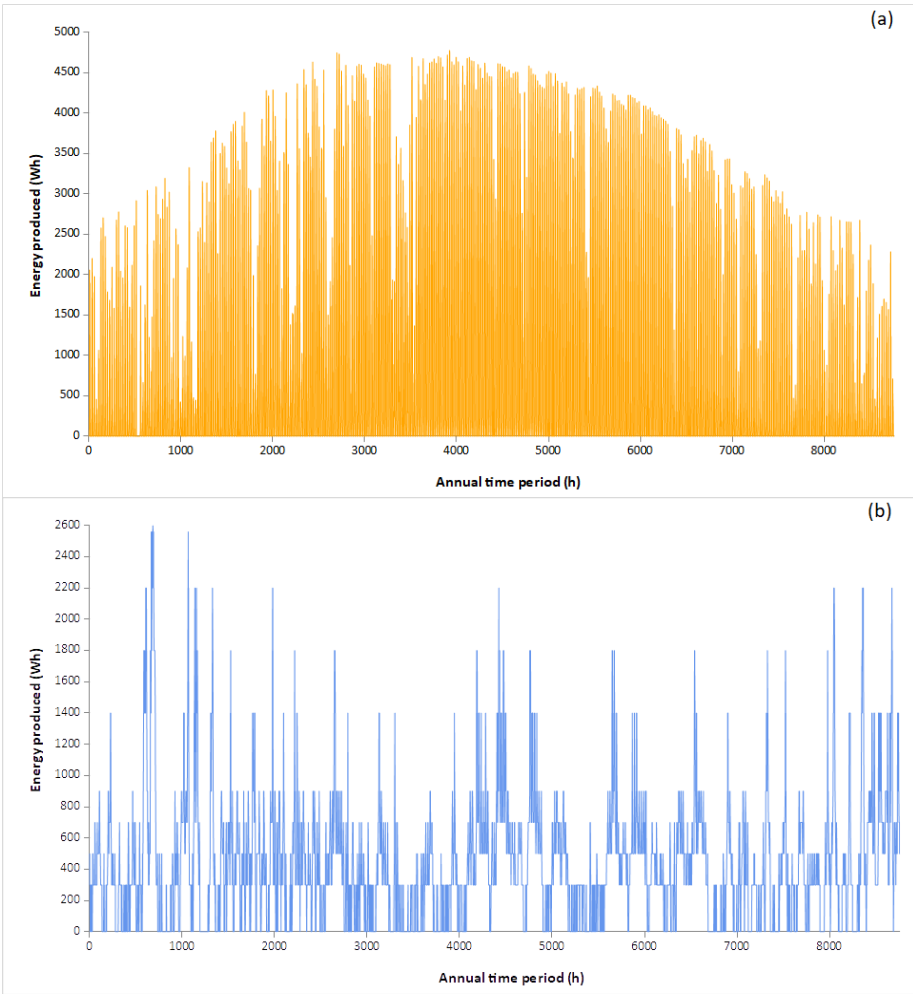

Figure 5. Time series of the energy produced by the optimal configuration from (**a**) photovoltaics and (**b**) wind turbines.

The distribution of the produced electricity can be seen in detail in the hourly time series displayed in Figure 5. The production of the photovoltaic array follows very closely the distribution of the solar irradiance presented in Section 2. The contribution of the wind turbine during the winter, when the production of the photovoltaic array is lower, is clearly shown.

As shown in the figures, the energy electricity via the hybrid system is not constant, due to the intermittence of the solar and wind resources. The demand is covered by the energy storage during hours of low generation. The energy stored in the micro-CAES or batteries is shown in Figures 6 and 7, respectively, for the month of December. The system operated for 660 h in December, while the average monthly operation was 608 h. It can be seen that energy supplied by the batteries is, for several hours, lower than the energy supplied by the micro-CAES system. This can be explained by the higher depth of discharge of the micro-CAES, compared with that of the batteries. A low depth of discharge is required for a higher number of cycles in the battery. An amount of energy E_s was stored, while another E_{unused} was unused during the year, as calculated by Equation (17). In the optimal scenario, the annual stored energy was 8709 kWh and 8595 kWh for micro-CAES and batteries, respectively.

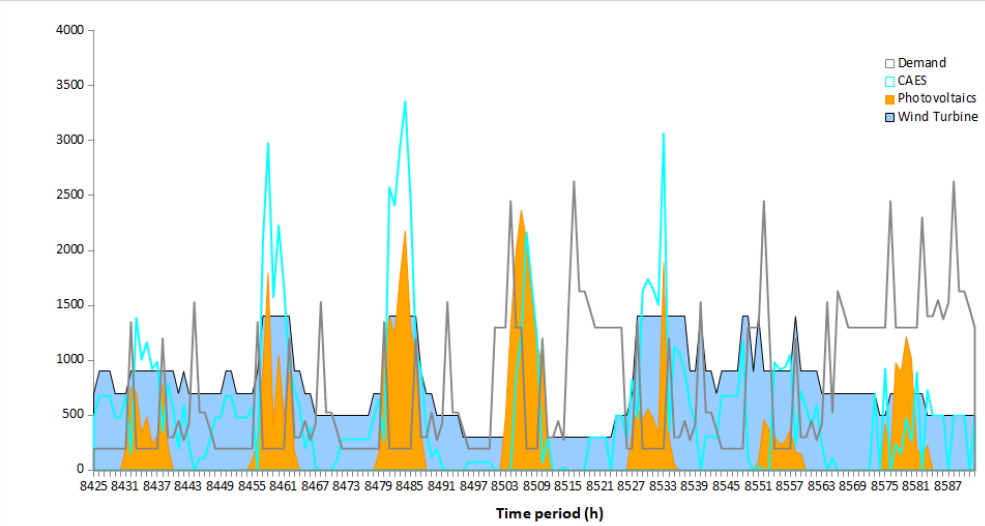

Figure 6. Energy produced by the system with micro-CAES during December.

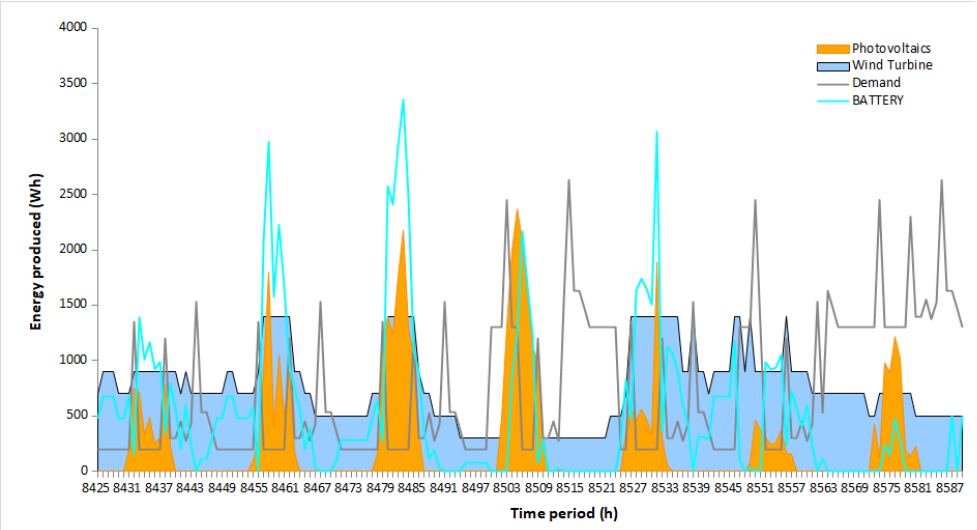

Figure 7. Energy produced by the system with batteries during December.

4. Discussion

The modeled energy storage with micro-CAES overcomes the constraints of large scale CAES plants, with their dependence on underground storage, and micro-CAES is suitable for distributed generation, suggesting the possible application of the presented methodology in different locations around the world. Further consideration of the associated costs is subject to energy market pricing. Recent progress in mixed-integer linear programming [34] and virtual power plants [35] has led to promising approaches toward this end.

The installation of small wind turbines in urban residences may cause unwanted disturbance. However, it was shown that the electricity produced by a wind turbine temporally complements the electricity produced by photovoltaics. In addition, there are advantages in the use of small-scale generators in the absence of a suitable morphology for solar power and large-scale wind turbines [36], as well as in distributed generation via energy communities [37]. Consequently, in rural areas outside the urban environment, a combination of small-scale wind and rooftop solar photovoltaics is sensible. A combination of 2/30 wind turbines/photovoltaic panels was found to be the optimal ratio for an LOLP of 2% (see Table 2).

The presented algorithm follows an isentropic compression and expansion [23]. The proposal of [38] of using the basic Ericsson cycle, by removing the high-pressure compressor and expander, offers a simpler structure with fewer components and less maintenance. The residential utility of micro-CAES involves a compact overall structure of the system, featuring stand-alone reliability and the embodiment of distributed generation. If the high-pressure components are removed, the system works at higher temperatures in a low-pressure turbine [14]. The proposed implementation of the basic Ericsson cycle is, nevertheless, closer to an isothermal process, which is more efficient than an adiabatic process following the Brayton cycle. Before expansion in the turbine, the compressed air can be heated to obtain up to three times more power [38]. This is achieved more efficiently in conjunction with a gas turbine, where 50–60% savings in the total consumed energy can be achieved [13]. Moreover, if the cooling effect is used directly for space cooling, the aggregated energy can be used more efficiently. A CAES refrigeration system is more efficient than a vapor compression refrigeration system that is widely used for space cooling [39]. In this way, coverage of space heating and cooling can be achieved, while the integration of micro-CAES units in residential scale, in addition to electricity production, can achieve more effective usage of the technology [39].

At the moment, the use of high-pressure vessels made of steel is an instant solution, but the manufacturing of such tanks is not cost-effective. Research and development for new enhanced materials, such as new composite fibers and thermoplastics [40], support investigation into the lower costs of reinforced vessels [41].

The CAES conservation load-shape objective, along with the six well-known load-shape objectives, is predicted to cover the demand, increase the storage fraction, and keep the power generation of the region at lower levels. Thermal energy storage was also used for demand-side management; however, it is limited to space heating. The energy-storage objective of demand-side management programs has successfully achieved reduced demand in space heating and, as a consequent result, partly reduced electricity consumption. If the direct use of thermal storage for electrical energy storage is not an option, the use of alternative methods of energy storage, such as micro-CAES, can spread widely and assist in power generation.

5. Conclusions

Integrating energy storage in renewable energy technologies enables energy usage later in the day during peak demand hours. In this way, equalizing the intermittency of renewable energy and technology can achieve more efficient usage of renewable resources. In the presented model, a number of criteria-based scenarios were investigated and compared to obtain an LOLP of 2%. An optimal configuration of 30 photovoltaic panels and

two wind turbines was found for micro-CAES or battery storage. This resulted in an annual energy production of 11.87 MWh. The annual stored energy of micro-CAES was 114 kWh higher than that of the system with batteries which, in addition to the lower cost and longer lifetime compared to batteries, makes micro-CAES a reasonable energy storage option for demand management.

Author Contributions: Conceptualization, investigation, data curation, writing—original draft preparation, G.E.A.; methodology, software, G.E.A.; writing—review and editing, G.E.A., G.K.-O. and D.A.K. All authors have read and agreed to the published version of the manuscript.

Funding: This research received no external funding.

Data Availability Statement: Not applicable.

Acknowledgments: M. Theristis and A. Phinikarides are acknowledged for input and help with the development of the algorithm of the presented model. G.E.A. appreciates the academic scholarship of the postdoctoral program in HMU that supported this work.

Conflicts of Interest: The authors declare no conflict of interest.

Nomenclature

CSP	Concentrated solar power
BOS	Balance of system
CAES	Compressed sir energy storage
LFG	Landfill gas
LOLP	Loss of load probability
O&M	Operation and maintenance
TACAS	Thermal and compressed air storage
SSCAES	Small subsurface compressed air energy storage
UPS	Uninterruptible power supply
C_B	Battery capacity
DOD	Depth of discharge
$E_{dem}(j)$	Energy load demand
$E_{user}(j)$	Energy supplied to the user
$E_U(j)$	Unsatisfied energy
$E_S(j)$	Energy for storage
$E_{unused}(j)$	Unused energy
SOS(j)	State of storage at j hour
η_{inv}	Efficiency of inverter
η_{bat}	Efficiency of battery
η_c	Efficiency of compression and expansion

References

1. Solar PV—Analysis. Available online: https://www.iea.org/reports/solar-pv (accessed on 24 November 2022).
2. Arnaoutakis, G.E.; Katsaprakakis, D.A.; Christakis, D.G. Dynamic Modeling of Combined Concentrating Solar Tower and Parabolic Trough for Increased Day-to-Day Performance. *Appl. Energy* **2022**, *323*, 119450. [CrossRef]
3. Ziyati, D.; Dollet, A.; Flamant, G.; Volut, Y.; Guillot, E.; Vossier, A. A Multiphysics Model of Large-Scale Compact PV–CSP Hybrid Plants. *Appl. Energy* **2021**, *288*, 116644. [CrossRef]
4. Manley, P.; Segantini, M.; Ahiboz, D.; Hammerschmidt, M.; Arnaoutakis, G.; MacQueen, R.W.; Burger, S.; Becker, C. Double-Layer Metasurface for Enhanced Photon up-Conversion. *APL Photonics* **2021**, *6*, 036103. [CrossRef]
5. Arnaoutakis, G.E.; Katsaprakakis, D.A. Concentrating Solar Power Advances in Geometric Optics, Materials and System Integration. *Energies* **2021**, *14*, 6229. [CrossRef]
6. Mahon, N.S.; Korolik, O.V.; Khenkin, M.V.; Arnaoutakis, G.E.; Galagan, Y.; Soriūtė, V.; Litvinas, D.; Ščajev, P.; Katz, E.A.; Mazanik, A.V. Photoluminescence Kinetics for Monitoring Photoinduced Processes in Perovskite Solar Cells. *Sol. Energy* **2020**, *195*, 114–120. [CrossRef]
7. Arnaoutakis, G.E.; Kefala, G.; Dakanali, E.; Katsaprakakis, D.A. Combined Operation of Wind-Pumped Hydro Storage Plant with a Concentrating Solar Power Plant for Insular Systems: A Case Study for the Island of Rhodes. *Energies* **2022**, *15*, 6822. [CrossRef]
8. Cole, W.; Frazier, A.W.; Augustine, C. *Cost Projections for Utility-Scale Battery Storage: 2021 Update*; National Renewable Energy Lab. (NREL): Golden, CO, USA, 2021.

9. Gyuk, I. *EPRI-DOE Handbook of Energy Storage for Transmission and Distribution Applications*; EPRI, Palo Alto, CA, and the U.S. Department of Energy: Washington, DC, USA, 2003; p. 1001834.
10. Katsaprakakis, D.A. 15-Energy Storage for Offshore Wind Farms. In *Offshore Wind Farms*; Ng, C., Ran, L., Eds.; Woodhead Publishing: Sawston, UK, 2016; pp. 459–493. ISBN 978-0-08-100779-2.
11. Mason, J.; Fthenakis, V.; Zweibel, K.; Hansen, T.; Nikolakakis, T. Coupling PV and CAES Power Plants to Transform Intermittent PV Electricity into a Dispatchable Electricity Source. *Prog. Photovolt. Res. Appl.* **2008**, *16*, 649–668. [CrossRef]
12. Shan, R.; Reagan, J.; Castellanos, S.; Kurtz, S.; Kittner, N. Evaluating Emerging Long-Duration Energy Storage Technologies. *Renew. Sustain. Energy Rev.* **2022**, *159*, 112240. [CrossRef]
13. Farret, F.A.; Simoes, M.G. *Integration of Alternative Sources of Energy*; John Wiley & Sons: Hoboken, NJ, USA, 2006; ISBN 978-0-471-75561-6.
14. Succar, S.; Williams, R.H. Compressed Air Energy Storage: Theory, Resources, and Applications for Wind Power. *Princet. Environ. Inst. Rep.* **2008**, *8*, 81.
15. Nakhamkin, M.; Wolk, R.H.; van der Linden, S.; Patel, M. *New Compressed Air Energy Storage Concept Improves the Profitability of Existing Simple Cycle, Combined Cycle, Wind Energy, and Landfill Gas Power Plants*; American Society of Mechanical Engineers Digital Collection: Vienna, Austria, 2008; pp. 103–110.
16. Struckmeier, W.; Richts, A. WHYMAP and the World Map of Transboundary Aquifer Systems at the Scale of 1:50,000,000 (Special Edition for the 4th World Water Forum, Mexico City, March 2006). *Epis. J. Int. Geosci.* **2006**, *29*, 274–278. [CrossRef]
17. Guo, C.; Li, C.; Zhang, K.; Cai, Z.; Ma, T.; Maggi, F.; Gan, Y.; El-Zein, A.; Pan, Z.; Shen, L. The Promise and Challenges of Utility-Scale Compressed Air Energy Storage in Aquifers. *Appl. Energy* **2021**, *286*, 116513. [CrossRef]
18. DTI, D. Status of Electrical Energy Storage Systems. *Rep. DTI (Dep. Trade Ind.)* **2004**.
19. Active Power, Austin, Texas; Group, S.M. Thermal and Compressed-Air Storage System Provides Alternative to UPS Batteries. Available online: https://www.techbriefs.com/component/content/article/tb/pub/briefs/mechanics-and-machinery/332 (accessed on 28 October 2022).
20. Congedo, P.M.; Baglivo, C.; Panico, S.; Mazzeo, D.; Matera, N. Optimization of Micro-CAES and TES Systems for Trigeneration. *Energies* **2022**, *15*, 6232. [CrossRef]
21. Anierobi, C.C.; Bhattacharya, K.; Canizares, C.A. Behind-the-Meter Compressed Air Energy Storage Feasibility and Applications. *Electr. Power Syst. Res.* **2020**, *189*, 106630. [CrossRef]
22. Thanos, D.; Maragkaki, A.; Venieri, D.; Fountoulakis, M.; Manios, T. Enhanced Biogas Production in Pilot Digesters Treating a Mixture of Olive Mill Wastewater and Agro-Industrial or Agro-Livestock By-Products in Greece. *Waste Biomass Valor* **2021**, *12*, 135–143. [CrossRef]
23. Castellani, B.; Morini, E.; Nastasi, B.; Nicolini, A.; Rossi, F. Small-Scale Compressed Air Energy Storage Application for Renewable Energy Integration in a Listed Building. *Energies* **2018**, *11*, 1921. [CrossRef]
24. Romero-Fiances, I.; Livera, A.; Theristis, M.; Makrides, G.; Stein, J.S.; Nofuentes, G.; de la Casa, J.; Georghiou, G.E. Impact of Duration and Missing Data on the Long-Term Photovoltaic Degradation Rate Estimation. *Renew. Energy* **2022**, *181*, 738–748. [CrossRef]
25. Theristis, M.; Livera, A.; Micheli, L.; Ascencio-Vásquez, J.; Makrides, G.; Georghiou, G.E.; Stein, J.S. Comparative Analysis of Change-Point Techniques for Nonlinear Photovoltaic Performance Degradation Rate Estimations. *IEEE J. Photovolt.* **2021**, *11*, 1511–1518. [CrossRef]
26. Theristis, M.; Stein, J.S.; Deline, C.; Jordan, D.; Robinson, C.; Sekulic, W.; Anderberg, A.; Colvin, D.J.; Walters, J.; Seigneur, H.; et al. Onymous Early-Life Performance Degradation Analysis of Recent Photovoltaic Module Technologies. *Prog. Photovolt. Res. Appl.* **2022**. [CrossRef]
27. Früh, W.-G. From Local Wind Energy Resource to National Wind Power Production. *AIMSE* **2015**, *3*, 101–120. [CrossRef]
28. Theristis, M.; Papazoglou, I.A. Markovian Reliability Analysis of Standalone Photovoltaic Systems Incorporating Repairs. *IEEE J. Photovolt.* **2014**, *4*, 414–422. [CrossRef]
29. Arnaoutakis, G.E.; Papadakis, N.; Katsaprakakis, D. CombiCSP: A Python Routine for Dynamic Modeling of Concentrating Solar Power Plants. *Softw. Impacts* **2022**, *13*, 100367. [CrossRef]
30. Früh, W.-G.; Trigg, C.; Jacob, R. A Model for Optimum Prioritisation of Energy Storage Use. I: Optimum Local Use of Local Generation. *REPQJ* **2022**, *20*, 301–306. [CrossRef]
31. Huld, T.; Müller, R.; Gambardella, A. A New Solar Radiation Database for Estimating PV Performance in Europe and Africa. *Sol. Energy* **2012**, *86*, 1803–1815. [CrossRef]
32. Panayiotou, G.; Kalogirou, S.; Tassou, S. Design and Simulation of a PV and a PV–Wind Standalone Energy System to Power a Household Application. *Renew. Energy* **2012**, *37*, 355–363. [CrossRef]
33. Katsaprakakis, D.A.; Papadakis, N.; Christakis, D.G.; Zervos, A. On the Wind Power Rejection in the Islands of Crete and Rhodes. *Wind Energy* **2007**, *10*, 415–434. [CrossRef]
34. Nikolakakis, T.; Fthenakis, V. Compressed Air Energy Storage Models for Energy Arbitrage and Ancillary Services: Comparison Using Mixed Integer Programming Optimization with Market Data from the Irish Power System. *Energy Technol.* **2018**, *6*, 1290–1301. [CrossRef]
35. Hany Elgamal, A.; Kocher-Oberlehner, G.; Robu, V.; Andoni, M. Optimization of a Multiple-Scale Renewable Energy-Based Virtual Power Plant in the UK. *Appl. Energy* **2019**, *256*, 113973. [CrossRef]

36. Katsaprakakis, D.A.; Dakanali, I.; Condaxakis, C.; Christakis, D.G. Comparing Electricity Storage Technologies for Small Insular Grids. *Appl. Energy* **2019**, *251*, 113332. [CrossRef]
37. Katsaprakakis, D.A.; Proka, A.; Zafirakis, D.; Damasiotis, M.; Kotsampopoulos, P.; Hatziargyriou, N.; Dakanali, E.; Arnaoutakis, G.; Xevgenos, D. Greek Islands' Energy Transition: From Lighthouse Projects to the Emergence of Energy Communities. *Energies* **2022**, *15*, 5996. [CrossRef]
38. Kim, Y.M.; Favrat, D. Energy and Exergy Analysis of a Micro-Compressed Air Energy Storage and Air Cycle Heating and Cooling System. *Energy* **2010**, *35*, 213–220. [CrossRef]
39. Wang, S.; Chen, G.; Fang, M.; Wang, Q. A New Compressed Air Energy Storage Refrigeration System. *Energy Convers. Manag.* **2006**, *47*, 3408–3416. [CrossRef]
40. Papadakis, N.; Reynolds, N.; Pharaoh, M.W.; Wood, P.K.C.; Smith, G.F. Strain Rate Dependency of the Shear Properties of a Highly Oriented Thermoplastic Composite Material Using a Contacting Displacement Measurement Methodology—Part B: Shear Damage Evolution. *Compos. Sci. Technol.* **2004**, *64*, 739–748. [CrossRef]
41. Baker, J. New Technology and Possible Advances in Energy Storage. *Energy Policy* **2008**, *36*, 4368–4373. [CrossRef]

Disclaimer/Publisher's Note: The statements, opinions and data contained in all publications are solely those of the individual author(s) and contributor(s) and not of MDPI and/or the editor(s). MDPI and/or the editor(s) disclaim responsibility for any injury to people or property resulting from any ideas, methods, instructions or products referred to in the content.